Title

Large Negative-Thermal-Quenching Effect in Phonon-Induced Light Emissions in Mn4+-Activated Fluoride Phosphor for Warm-White Light-Emitting Diodes

Permalink

https://escholarship.org/uc/item/8rr652c2

Journal

ACS Omega, 3(10)

ISSN

2470-1343

Authors

Tang, Fei

Su, Zhicheng

Ye, Honggang

et al.

Publication Date

2018-10-31

DOI

10.1021/acsomega.8b01127

Large Negative-Thermal-Quenching Effect in Phonon-Induced Light Emissions in Mn^{4+}-Activated Fluoride Phosphor for Warm-White Light-Emitting Diodes

Fei Tang,[†,§] Zhicheng Su,[†,∥] Honggang Ye,[†,⊥] Wenpei Gao,[‡] Xiaoqing Pan,[‡] and Shijie Xu*,[†]

[†]Department of Physics and Shenzhen Institute of Research and Innovation (HKU-SIRI), The University of Hong Kong, Pokfulam Road, Hong Kong, China

[‡]Department of Materials Science & Engineering, University of California−Irvine, Irvine, California 92697, United States

ABSTRACT: Currently, hunting for anti-temperature-degradation high-efficiency phosphors has become crucially significant for fabricating high-brightness phosphor-converted white light-emitting diodes (pc-WLEDs). Herein, we show that photoluminescence in a kind of full-solution-processed K$_2$SiF$_6$:Mn^{4+} red phosphor exhibits an extraordinarily large negative thermal quenching property. For instance, under the excitation of 477 nm laser light, the sample photoluminescence intensity amazingly increases by 347-fold when the temperature is increased from 4 to 477 K. The temperature-driven transition probability enhancement of the phonon-induced luminescence around Mn^{4+} ions in the phosphor is argued to be responsible for the large negative-thermal-quenching phenomenon. We also demonstrate a pc-WLED with R_a of 82 and correlated color temperature of 2701 K by using the K$_2$SiF$_6$:Mn^{4+} red phosphor + commercial yellow phosphor of YAG:Ce^{3+}.
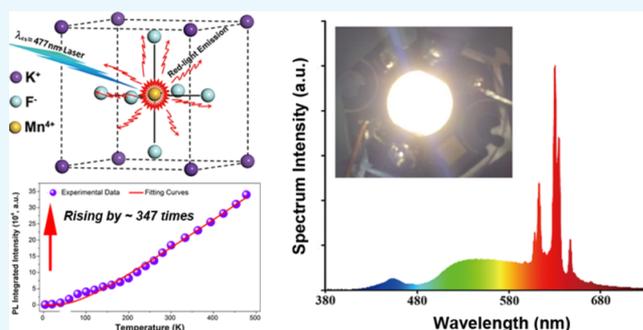
INTRODUCTION

Solid-state light-emitting diode (LED) lighting technology triggered by the discovery of efficient blue LEDs offers the most promising change in lighting technology since Edison created the first commercialized electrical lightbulb over 130 years ago.[1,2] In sharp contrast to the electrical "hot" lightbulbs, emerging LED lightbulbs belong to so-called "cold" light sources. Great energy saving and environmental friendship are the most favored advantages of LED-based cold lightbulbs.[3] Among the already-demonstrated white light LED bulbs, InGaN blue LED chip + high-efficiency luminescent phosphor forms a mainstream module, and has been even specially termed as phosphor-converted white LED (pc-WLED).[4] In such a module, phosphors play a crucial role in determining the performance and quality of pc-WLED. In turn, the development of pc-WLED lightbulbs puts forward greater demands on phosphors for luminescence quantum efficiency and simultaneous thermal stability. Unfortunately, almost all the existing solid luminescent materials suffer from severe degradation in emission intensity and even thermal quenching with the rise of temperature.[5−11] Such thermal deterioration of emission intensity is mainly ascribed to the rapid increase of nonradiative multiphonon transition probability with temperature. Presently, hunting for high-efficiency and anti-temperature-degradation phosphors has become a key challenge for fabricating high-brightness pc-WLED lightbulbs.[12,13] Very recently, Kim and his co-workers reported a zero-thermal-quenching blue phosphor of Na$_{3−2x}$Sc$_2$(PO$_4$)$_3$:xEu^{2+} phosphor

that does not exhibit thermal quenching even up to 200 °C.[13] The zero-thermal-quenching phenomenon is explained by them as polymorphic modification and possible energy transfer from electron−hole pairs at the thermally activated defect levels to the Eu^{2+} 5d-band with increasing temperature. This important finding also inspires the exploration of converting phosphors with a zero-thermal-quenching and even a negative-thermal-quenching property for high-power LED applications.

In recent years, Mn^{4+}-activated inorganic phosphors have quickly emerged as a new class of promising phosphors for fabricating pc-WLED because of their high-efficiency narrow red-light emissions.[14−23] Among them is cubic K$_2$SiF$_6$:Mn^{4+} phosphor, which can be synthesized at −16 °C with a full-solution chemical route,[22] showing an outstanding property of phonon-induced dominant luminescence at room temperature.[25] In the present study, we report an observation and argument on large negative-thermal-quenching phenomenon in the cubic K$_2$SiF$_6$:Mn^{4+} phosphor for temperature variation from 4 to 477 K, when it was under the excitation of 477 nm nonintensive laser light. Such an amazing property makes the phosphor be disruptively different from the most luminescence solids whose luminescence intensities usually weaken with the rise of temperature and be appealing as a kind of thermal energy (phonons) converting phosphor for luminescence at

high temperatures. Together with the commercial yellow phosphor of YAG:Ce^{3+}, this kind of narrow red phosphor is utilized to convert a 450 nm InGaN blue chip into a warm white LED with good performance.

■ RESULTS AND DISCUSSION

As mentioned earlier, cubic K$_2$SiF$_6$:Mn^{4+} phosphor was synthesized at −16 °C with a full-solution approach. The detailed synthesis procedure has been described elsewhere.[22] For crystalline structure characterization on the synthesized phosphor, precise X-ray diffraction patterns and analysis can also be referred to in ref 24. Here, we present high-resolution transmission electron microscopy (HRTEM) characterization on the local microstructures of the K$_2$SiF$_6$:Mn^{4+} phosphor, as shown in Figure 1a. By selecting an area of about 160 × 160
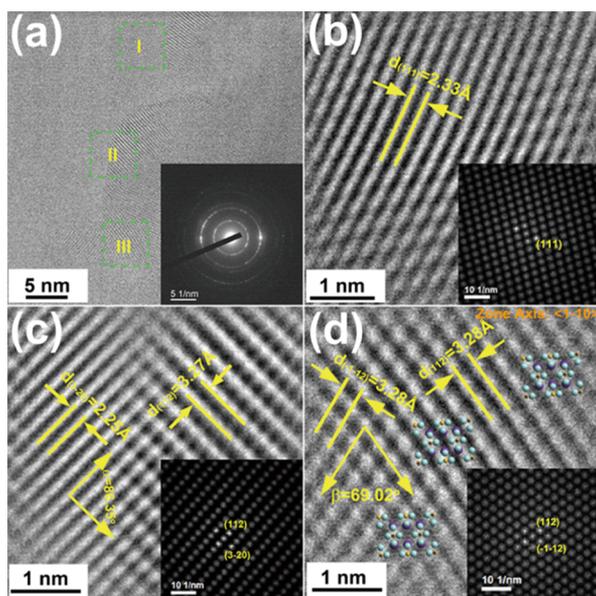
Figure 1. (a) HRTEM image of the K$_2$SiF$_6$:Mn^{4+} phosphor. The inset shows the selected area electronic diffraction patterns. (b−d) enlarged HRTEM regions (I−III) in (a), respectively, and their corresponding FFT patterns.

nm^2 as the diffraction region, we completed an electron diffraction experiment. The inset shows the electron diffraction patterns composed of spotted circles, indicating the crystalline nature of the phosphor. In order to obtain a closer inspection on the lattice structures of the crystalline phosphor, three regions [e.g., (I), (II), and (III) in Figure 1a were enlarged and re-illustrated in (b), (c), and (d), respectively. Their corresponding fast Fourier transformation (FFT) patterns are depicted at the bottom corners of the respective figures. Several lattice plane spacings and lattice structural angles were determined, as shown in Figure 1b−d. In spite of the limited resolution, the cubic lattice structure of the phosphor can be certainly verified in the local enlarged HRTEM image, as marked in Figure 1c.

Figure 2a shows photoluminescence (PL) spectra of the K$_2$SiF$_6$:Mn^{4+} phosphor measured at different temperatures. A remarkable increase of the red emission intensity with temperature may be more straightforwardly seen in photographs in Figure 2b. For the temperature increase from 4 to 477 K, the color of photographs changes from bright blue largely because of the Rayleigh scattering of the 477 nm
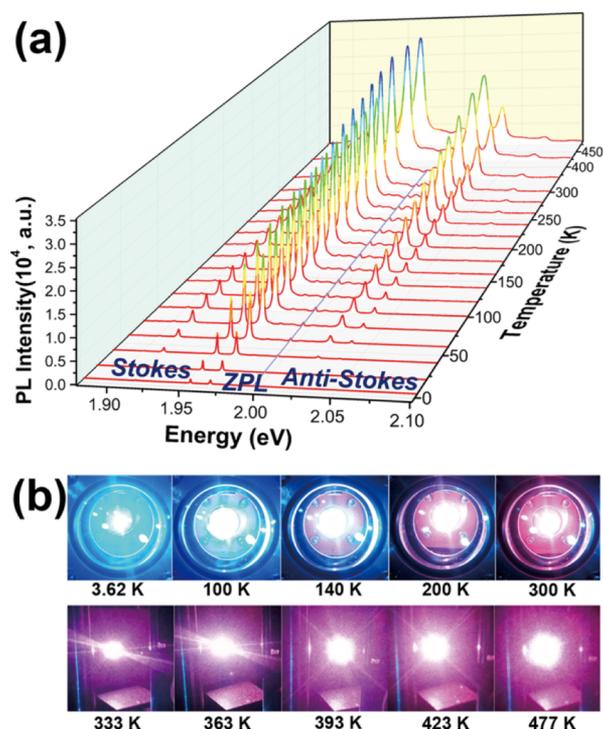
Figure 2. (a) PL spectra of the phosphor measured at different temperatures under the excitation of 477 nm laser light; (b) PL photographs of the sample at various temperatures.

excitation light by the powder sample to dazzling red because of amazing enhancement of the red emission of the sample. As seen from the PL spectra, instead of the magnetic-dipole transition-induced zero-phonon line (ZPL),[25] the luminescence (phonon sidebands) around the Mn^{4+} ion by the electric-dipole transitions is always dominant in the PL spectra of the phosphor. It has been identified that the vibronic states arising from the coupling of ^2E_g excited state of Mn^{4+} ions with the three triplet odd-parity vibration modes (ν_3, ν_4, and ν_6) of the host lattice are responsible for the three main emission bands including both Stokes and anti-Stokes bands.[22,24,26] Disappearance of the ZPL line reflects both the spin- and parity-forbidden nature of the electronic transitions between ^2E_g and $^4A_{2g}$ electronic states of Mn^{4+} ions in a cubic K$_2$SiF$_6$ lattice. It is known that in a perfect K$_2$SiF$_6$ single crystal with cubic structure, a Si^{4+} ion is tightly coordinated with six nearest F$^-$ ions, constituting a perfect octahedral structure with local inversion symmetry of point group O_h.[26,27] When Mn atoms are intentionally incorporated into this host matrix to replace Si, a new octahedral structure of [MnF$_6$]$^{2-}$ with some lattice distortion but remaining the inversion symmetry forms.[26−29] The new octahedral structure of [MnF$_6$]$^{2-}$ may belong to a point group of D_{4h}.[29−32] In the host crystal, [MnF$_6$]$^{2-}$ can act as an efficient luminescence center.[12,20,21] Probably, an outstanding property of this luminescence center is that its emission intensity rises so strongly with increasing the temperature, as seen in Figure 3a where the overall integrated PL intensity (solid circles + dashed line) versus temperature is illustrated. For example, the total emission intensity amazingly rises by ∼347-fold when the temperature is increased from 4 to 477 K. The blue solid line represents a theoretical fitting curve with eq 1, which is an analytical expression approximately based on relevant theoretical models[26,33−36]
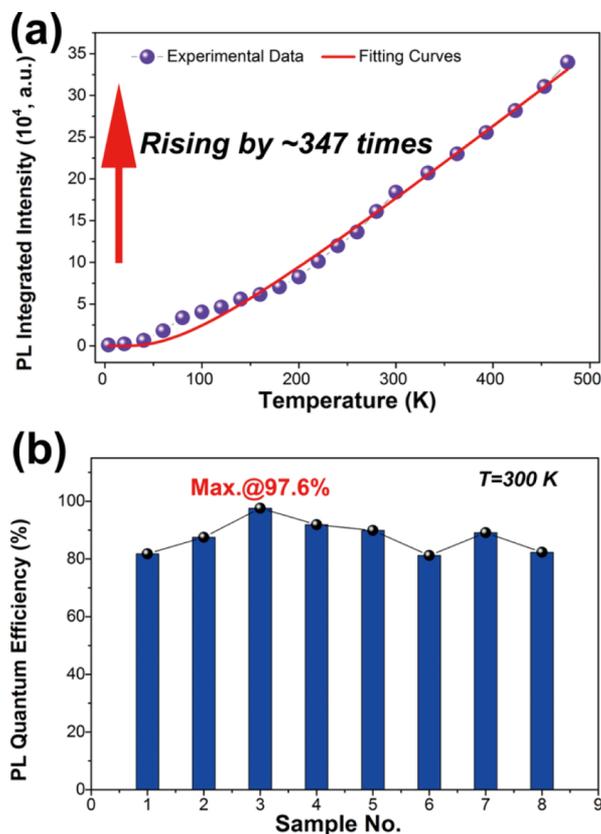
Figure 3. (a) Total PL integrated intensities (solid circles + solid line) vs temperature; (b) PL QYs of the sample measured at room temperature.

$$P(T) = C \frac{\exp(-\Delta E / k_B T)}{\exp(\hbar \omega_v / k_B T) - 1} \quad (1)$$

where C is a constant, ΔE an energy separation with respect to the ZPL, $\hbar \omega_v$ an average characteristic energy of involved phonons, and k_B the Boltzmann constant. In fact, $1/[\exp(\hbar\omega_v/k_B T) - 1]$ in eq 1 represents the Bose−Einstein distribution of the involved phonons.

In order to understand the remarkable enhancement of the PL intensity in the interested temperature range, we measured the PL excitation (PLE) spectra of the sample at different temperatures, as shown in Figure 4. It is obvious that the PLE intensity at 477 nm increases substantially with increasing the temperature. The consistent enhancement in both PL and PLE signals unambiguously indicates the occurrence of a negative-thermal-quenching effect in the studied K_2SiF_6:Mn^{4+} phosphor. The major mechanism of the negative-thermal-quenching effect in the studied K_2SiF_6:Mn^{4+} phosphor with cubic structure shall be the nature of phonon-induced radiative transitions at Mn^{4+} ions which strictly occupy the inversion center with surrounding six nearest F^- ions, as shown in Figure 5a. Such central inversion symmetry directly leads to a forbidden pure $^2E_g \rightarrow {}^4A_{2g}$ transition of Mn^{4+} ions according to the Laporte rule. This rule states that the d−d electronic transitions in atoms in a centrosymmetric environment are electric-dipole-forbidden, which applies to octahedral coordination compounds of the transition metals.[37] A zero or extremely weak ZPL line is indeed observed in the experiment. On the contrary, the phonon-assisted $^2E_g \rightarrow {}^4A_{2g}$ transitions (vibronic transitions) may become dominant. In such vibronic
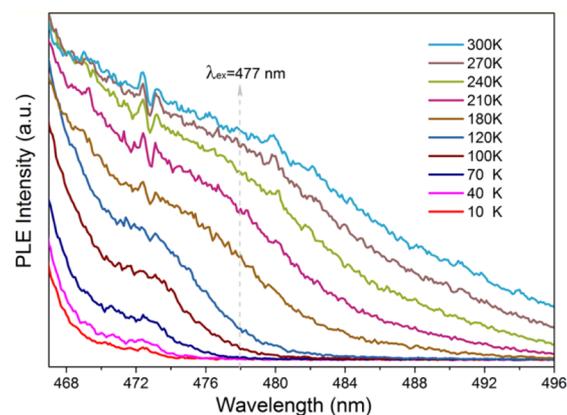
Figure 4. PLE spectra measured in the spectral range of 467−496 nm at various temperatures. Clearly, the PLE intensity at 477 nm increases significantly with the rise of temperature.
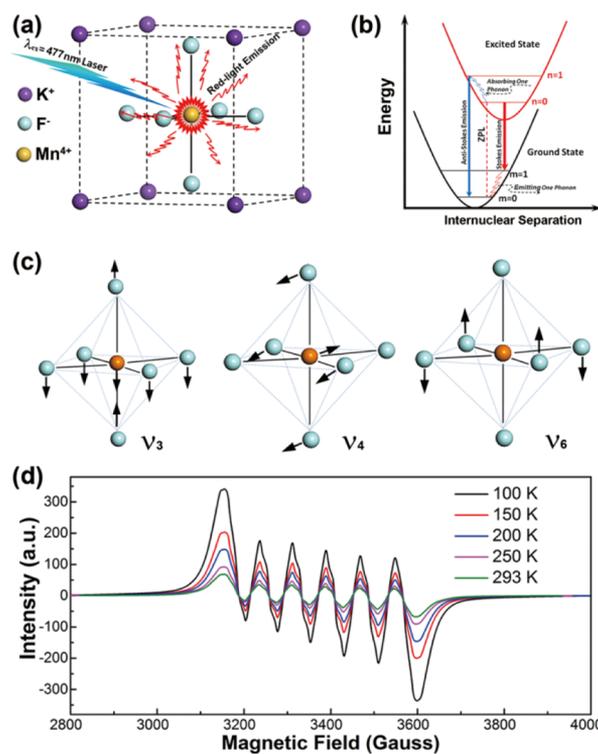
Figure 5. (a) Schematic diagram of a face-centered cubic structure containing an octahedral luminescence center of Mn^{4+}. Red-light emission occurs around Mn^{4+} ions under the excitation of a 477 nm blue laser beam. (b) Configurational coordinate diagram for radiative transitions around Mn^{4+} ions in a K_2SiF_6 host crystal. (c) Three dominant phonon modes engaged in the electron−phonon coupling and vibronic transitions. (d) EPR spectra of K_2SiF_6:Mn^{4+} measured at various temperatures.

transitions, some phonons with particular symmetries (i.e., modes) play an essential role. On the basis of available theoretical studies,[26,33−36] we derived an approximated expression for the transition probability of vibronic transitions, as formulated by eq 1. This expression tells us that the transition probability depends distinctively on temperature, that is, roughly exponentially grows with temperature and hence thermal energy (e.g., $k_B T$). As shown in Figure 3a, remarkable enhancement is indeed observed for the total PL intensity of the K_2SiF_6:Mn^{4+} phosphor as the temperature
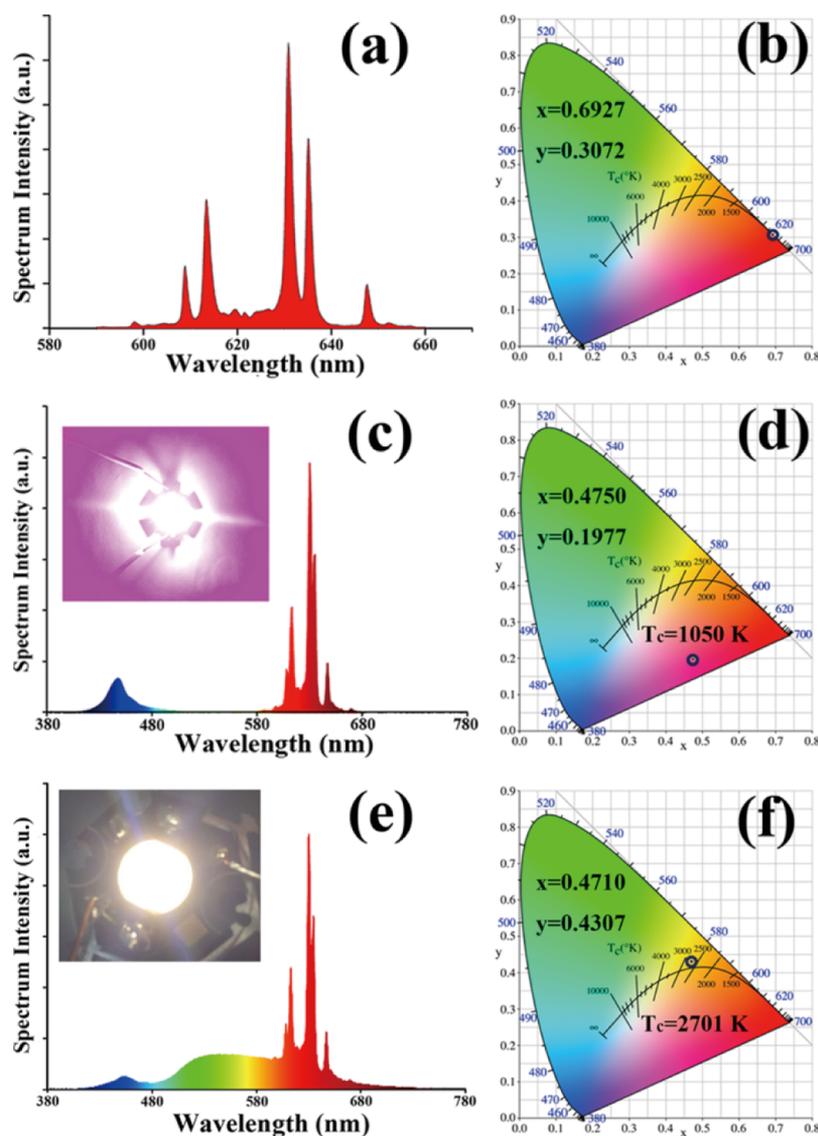
Figure 6. (a) Room-temperature PL spectrum of the $K_2SiF_6:Mn^{4+}$ phosphor alone. (b) CIE chromaticity coordinates of the PL spectrum in (a). (c) Room-temperature luminescence spectrum of a pc-WLED consisting of an InGaN blue LED and $K_2SiF_6:Mn^{4+}$ nanophosphor. (d) CIE chromaticity coordinates of the luminescence spectrum in (c). (e) Room-temperature luminescence spectrum of a pc-WLED made of an InGaN blue LED and the mixture of $K_2SiF_6:Mn^{4+}$ red phosphor + commercial YAG:Ce^{3+} yellow phosphor. (f) CIE chromaticity coordinates of the luminescence spectrum in (e). Note that the driving electric current of the pc-WLEDs was 60 mA.

increases. Moreover, good agreement between theory and experiment is achieved. In fact, temperature-induced enhancement of vibronic transitions has been repeatedly observed in the luminescence of analogous Cr^{3+} ions in garnet crystal,[38] phosphor[39] and transparent ceramics.[25]

We randomly selected eight $K_2SiF_6:Mn^{4+}$ specimens and measured their PL quantum yields (QYs) at room temperature. The results are illustrated in Figure 3b. It can be seen that all eight specimens have QY values above 80%, and the best one even higher than 97%.

As argued earlier and schematically illustrated in Figure 5a, a central Mn^{4+} ion tightly binds with six nearest F^- ions to form an octahedral luminescence center $[MnF_6]^{2-}$ in the cubic $K_2SiF_6:Mn^{4+}$ phosphor. Under the excitation of an appropriate light, for example, 477 nm blue laser, such a luminescence center can become excited via absorbing the incident photons and then emit red light by releasing the absorbed energy. For the absorptive and emissive optical transitions between the

vibronic states, a widely adopted picture, namely configurational coordinate model, is usually used to discuss them,[40,41] as schematically shown in Figure 5b. In the figure, the dashed vertical line represents a pure electronic transition which may produce the so-called ZPL line. In the studied case, such a "pure" electronic transition is a forbidden transition process because of both spin and parity transition rules. The bold red arrow denotes the Stokes radiative transition process accompanying the phonon emission, whereas the solid blue arrow stands for the anti-Stokes radiative transition in which phonon absorption is involved. For the $[MnF_6]^{2-}$ octahedral configuration, there are totally six main vibration modes, among which only three engage in the vibronic transitions. Figure 5c schematically illustrates the three vibration modes, that is, ν_3, ν_4, and ν_6. From the measured PL spectra, characteristic energies of phonons ν_6, ν_4, and ν_3 may be determined to be about 28.5, 41.4, and 78.7 meV, respectively. For the electronic part of the vibronic states, $3d^3$ electrons of

Mn^{4+} ions play a key role. To get more useful information on $3d^3$ electrons of Mn^{4+} ions in the studied phosphor, electron paramagnetic resonance (EPR) measurements were carried out at various temperatures under a fixed microwave frequency of 9.414×10^9 Hz. The experimental EPR data are illustrated in Figure 5d. From the figure, it can be seen that six main EPR signatures can be well detected, having g factors of 1.8−2.2. These six fine EPR structures exactly reflect the hyperfine interaction of $3d^3$ electrons of the Mn ion with the surrounding magnetic nucleus.[42] From the measured EPR data, that is, the spacing of two adjacent EPR structures, we may determine the hyperfine coupling constant. The obtained value of ∼80 Gauss is somewhat smaller than that of the $CaAl_{12}O_9$:Mn^{4+} (∼100 Gauss) phosphor probably because of the difference in local environment between the two different compounds.[43] Interestingly, the EPR signal intensity is observed to decline gradually with the rise of temperature. It is known that the EPR signal is proportional to the population difference between spin states of the defect.[43] The EPR signal decline with temperature may be mainly attributed to the decrease of population difference between the Zeeman states of Mn^{4+} ions because of the thermal distribution at higher spin states.

In the remainder of this paper, we examine the device performance of the K_2SiF_6:Mn^{4+} phosphor in pc-WLEDs. Room-temperature luminescence spectra of the phosphor alone and the two pc-WLEDs were measured, as shown in Figure 6. For the K_2SiF_6:Mn^{4+} phosphor powder, the International Commission on Illumination (CIE) chromaticity coordinates of the luminescence spectrum are calculated to be 0.6927 and 0.3072, located at the edge of the red region and marked by an open circle, as shown in Figure 6b. These results suggest that the red phosphors synthesized in this study are very suitable for the use of high-quality back-light display with wide color gamut. By combining it with a blue InGaN LED chip (luminescence peaking at 450 nm), a pink-light LED device can be formed, as shown in the inset figure of Figure 6c. The luminescence spectrum of this pc-WLED has coordinate positions at 0.4750 and 0.1977, and a relatively low correlated color temperature (CCT) of 1050 K. With further addition of commercial YAG:Ce^{3+} yellow phosphor, the measured luminescence spectrum of the new pc-WLED shows full-color emission behavior in the entire visible region, as seen in Figure 6e. The inset figure shows a photograph of the as-fabricated pc-WLED device. Chromaticity coordinates (0.4710, 0.4307) of the device are marked by an open circle in CIE color spaces in Figure 6f. Compared with the commercial pc-WLED with low color render index [color rendering index (CRI) or R_a < 70] and high CCT (>5000) only using YAG:Ce^{3+} yellow phosphor, we demonstrate a warm-white LED with excellent parameters, that is, R_a of 82 and CCT of 2701 K by adding the K_2SiF_6:Mn^{4+} phosphor as the red component phosphor. The obtained luminous efficiency of this pc-WLED is 124 lm/W under 60 mA driving current. The National Television System Committee (NTSC) value of the pc-WLED made of K_2SiF_6:Mn^{4+} + YAG:Ce^{3+} was measured to be about 45.34%. It is obvious that both the luminous efficiency and NTSC value of the demonstrated pc-WLED are not comparable to those of the latest commercial products.[44] Further process optimization in the fabrication of pc-WLED shall help improve the performance of the devices. It is of interest to note other demonstrated WLEDs, especially ones made of III-nitride nanowires on Si[45,46] and even on the Cu substrate.[47] For instance, Guo et al. demonstrated an InGaN/GaN disk-in-nanowire WLED with chromaticity coordinates of x = 0.29 and y = 0.37 and a CCT of 5500−6500 K at an injection current of 50 A/cm²,[45] whereas Philip et al. reported an InGaN/AlGaN nanowire WLED with a high CRI of ∼98.[46] More recently and interestingly, Philip et al. fabricated high-brightness phosphor-free III-nitride nanowire LEDs on Cu with highly stable white-light emission and high CRI of ∼95.[47] These studies may open another technical approach for fabricating phosphor-free WLEDs with high performance and some advantages such as more efficient thermal management and enhanced light-extraction efficiency.

■ CONCLUSIONS

In summary, the K_2SiF_6:Mn^{4+} phosphor synthesized at low temperature with a full-solution route is examined with emphasis on its variable-temperature PL property. The phosphor possesses good cubic crystalline structure evidenced by precise HRTEM images and the corresponding FFT patterns. More intriguingly, it exhibits an extraordinary thermally driven enhancement of emission intensity in a wide temperature range from 4 to 477 K under the excitation of a 477 nm weak laser. A significant increase of transition probability of the dominant vibronic transitions around Mn^{4+} ions with temperature is argued to be responsible for the observed negative thermal quenching. By combining this kind of phosphor with commercial YAG:Ce^{3+} yellow phosphor and 450 nm blue InGaN LED chip, we demonstrate a pc-WLED with good luminous properties.

■ EXPERIMENTAL DETAILS

Synthesis of the K_2SiF_6:Mn^{4+} Phosphor. The K_2SiF_6:Mn^{4+} phosphor was synthesized at a low temperature of −16 °C with a two-step wet-chemical method. In the first step, the K_2MnF_6 powder was prepared. For the preparation of the K_2MnF_6 powder, the KHF_2 powder was dissolved in HF solution first and then via strong stirring operation to form a uniform solution. By adding some amount of $KMnO_4$ powder into the solution, one obtained a black mixture solution. Followed by the addition of H_2O_2 solution, a brown-yellow solution was achieved with some precipitant generated. After three times of vacuum filtration and washing process, a drying process was carried out at 80 °C for one night before the brown K_2MnF_6 powder was obtained. In the second step, the obtained K_2MnF_6 powder was dissolved in the HF solution and gradually formed as a uniform golden-yellow solution during a vigorous stirring process. After the addition of KHF_2 powder, a continuous stirring operation was carried out until a uniform solution was achieved. H_2SiF_6 solution was then added dropwise into the above solution, and a golden-yellow precipitant was generated in the solution. Following three times of vacuum filtration and washing process, a drying operation was carried out at 80 °C for one night, and a final target product was prepared.

HRTEM Characterization. Precise structural characterization of the sample was carried out with HRTEM using a Jeol JEM-ARM300F TEM microscope. The microscope was operated at 300 kV with aberration correction for HRTEM imaging. As the specimen consisting of fluorine was sensitive to high-energy electron beam bombardment, HRTEM image-taking was done at a low electron dose <30 e/Å²·s. Images were acquired with Gatan OneView camera running at 25 (fps). Under such conditions, 25 frames were aligned using

cross correlation and integrated within 1 s to obtain a final image with the size of 4k × 4k.

High-Resolution PL Spectral Measurements. High-resolution PL spectra were recorded on a home-assembled PL setup using the 477 nm line of an Ar–Kr ion mixed gas laser (Coherent Innova-70) as the excitation source. In the variable-temperature PL measurements, the phosphor powder was mounted with silver paint on the cold finger of a closed cycle cryostat, providing a varying temperature range of 4–300 K. For the PL measurements at temperatures higher than 300 K, the phosphor sample was directly heated by a heater in the atmospheric environment. The luminescence signal of the sample was dispersed by a monochromator with focal length of 0.75 m (Spex 750M) and detected with a photomultiplier tube (Hamamatsu R928). A lock-in amplifier (Stanford Research SR830) together with a standard optical chopper was employed to enhance the signal-to-noise ratio. Finally, a data-acquire module was used to convert the detector electrical signal into digital data that can be accepted by a computer. The control and data-taking software was encoded by us with LabVIEW.

Testing Equipment and Method of Quantum Yields. PL QYs of the phosphors were measured on an Edinburgh FLS920-s fluorescence spectrometer + integrating sphere system at room temperature.

EPR Spectral Characterization. EPR spectra were recorded on a Bruker-Biospin (E500) spectrometer with the spectral resolution of 1 kHz. Sample temperature was controlled by using a liquid nitrogen variable-temperature control system. EPR spectra were measured via applying a microwave radiation of 9.41×10^9 Hz and scanning an external magnetic field.

LED-Device Performance Characterization. Pc-WLED devices were prepared with a 450 nm InGaN blue chip + a coating layer of the mixed phosphor of red K_2SiF_6:Mn^{4+} and yellow YAG:Ce^{3+} powders. Two kinds of phosphors were completely mixed with each other in silicone, and the obtained mixture was then coated on the surface of the LED chips for producing pc-WLEDs. Device performance was evaluated by using an Edinburgh FLS920-s fluorescence spectrometer + integrating sphere system. The prepared pc-WLEDs were operated under a driving current of 60 mA at room temperature. Spectral intensity distribution of the devices was used to calculate their CCT and CRI. Luminous efficiency was determined by calculating the ratio of the measured luminous flux output and the input electrical power of the pc-WLEDs.

■ **AUTHOR INFORMATION**

Corresponding Author
*E-mail: sjxu@hku.hk (S.J.X.).

ORCID ◉
Wenpei Gao: 0000-0002-2776-2676
Xiaoqing Pan: 0000-0002-0965-8568
Shijie Xu: 0000-0001-6522-5778

Present Addresses
§Present address: Jiangsu Key Laboratory of Advanced Laser Materials and Devices, School of Physics and Electronic Engineering, Jiangsu Normal University, Xuzhou 221116, China

∥Present address: Laboratory of Solid State Physics and Magnetism, Department of Physics and Astronomy, KU Leuven, Celestijnenlaan 200D, 3001 Leuven, Belgium
⊥Present address: Department of Applied Physics, Xi'an Jiaotong University, Xi'an 710049, China

Author Contributions
S.J.X. conceived the project of phonon-induced luminescence in solids and supervised the study. F.T. synthesized the phosphors and performed the PL experiments. Z.C.S. and H.G.Y. participated in the PL measurements. W.P.G. and X.Q.P. did HRTEM measurements on the sample. F.T. and S.J.X. completed the data analysis and wrote the article. All the authors discussed and reviewed the article.

Notes
The authors declare no competing financial interest.

■ **REFERENCES**

(1) Nakamura, S. The roles of structural imperfections in InGaN-based blue light-emitting diodes and laser diodes. *Science* **1998**, *281*, 956–961.
(2) Pust, P.; Schmidt, P. J.; Schnick, W. A revolution in lighting. *Nat. Mater.* **2015**, *14*, 454–458.
(3) Nakamura, S.; Pearton, S.; Fasol, G. *The Blue Laser Diode: The Complete Story*; Springer-Verlag: Berlin Heideberg, 2000.
(4) Reineke, S. Complementary LED technologies. *Nat. Mater.* **2015**, *14*, 459–462.
(5) Okamoto, K.; Niki, I.; Shvartser, A.; Narukawa, Y.; Mukai, T.; Scherer, A. Surface-plasmon-enhanced light emitters based on InGaN quantum wells. *Nat. Mater.* **2004**, *3*, 601–605.
(6) Wiersma, D. S.; Cavalieri, S. A temperature-tunable random laser. *Nature* **2001**, *414*, 708–709.
(7) Green, M. A.; Zhao, J.; Wang, A.; Reece, P. J.; Gal, M. Efficient silicon light-emitting diodes. *Nature* **2001**, *412*, 805–808.
(8) Suyver, J. F.; Wuister, S. F.; Kelly, J. J.; Meijerink, A. Synthesis and Photoluminescence of Nanocrystalline ZnS:Mn^{2+}. *Nano Lett.* **2001**, *1*, 429–433.
(9) Bachmann, V.; Ronda, C.; Meijerink, A. Temperature Quenching of Yellow Ce^{3+} Luminescence in YAG:Ce. *Chem. Mater.* **2009**, *21*, 2077–2084.
(10) Cao, X. A.; LeBoeuf, S. F.; Rowland, L. B.; Yan, C. H.; Liu, H. Temperature-dependent emission intensity and energy shift in InGaN/GaN multiple-quantum-well light-emitting diodes. *Appl. Phys. Lett.* **2003**, *82*, 3614–3616.
(11) Wei, Z. F.; Xu, S. J.; Duan, R. F.; Li, Q.; Wang, J.; Zeng, Y. P.; Liu, H. C. Thermal quenching of luminescence from buried and surface InGaAs self-assembled quantum dots with high sheet density. *J. Appl. Phys.* **2005**, *98*, 084305.

(12) Pust, P.; Weiler, V.; Hecht, C.; Tücks, A.; Wochnik, A. S.; Henß, A.-K.; Wiechert, D.; Scheu, C.; Schmidt, P. J.; Schnick, W. Narrow-band red-emitting $Sr[LiAl_3N_4]:Eu^{2+}$ as a next-generation LED-phosphor material. *Nat. Mater.* **2014**, *13*, 891−896.

(13) Kim, Y. H.; Arunkumar, P.; Kim, B. Y.; Unithrattil, S.; Kim, E.; Moon, S.-H.; Hyun, J. Y.; Kim, K. H.; Lee, D.; Lee, J.-S.; Im, W. B. A zero-thermal-quenching phosphor. *Nat. Mater.* **2017**, *16*, 543−550.

(14) Zhu, H.; Lin, C. C.; Luo, W.; Shu, S.; Liu, Z.; Liu, Y.; Kong, J.; Ma, E.; Cao, Y.; Liu, R.-S.; Chen, X. Highly efficient non-rare-earth red emitting phosphor for warm white light-emitting diodes. *Nat. Commun.* **2014**, *5*, 4312.

(15) Peng, M.; Yin, X.; Tanner, P. A.; Brik, M. G.; Li, P. Site occupancy preference, enhancement mechanism and thermal resistance of Mn^{4+} red luminescence in $Sr_4Al_{14}O_{25}:Mn^{4+}$ for warm WLEDs. *Chem. Mater.* **2015**, *27*, 2938−2945.

(16) Lü, W.; Lv, W.; Zhao, Q.; Jiao, M.; Shao, B.; You, H. A Novel Efficient Mn^{4+} Activated $Ca_{14}Al_{10}Zn_6O_{35}$ Phosphor: Application in Red-Emitting and White LEDs. *Inorg. Chem.* **2014**, *53*, 11985−11990.

(17) Li, W.; Zhang, H.; Chen, S.; Liu, Y.; Zhuang, J.; Lei, B. Preparation and Properties of Carbon Dot-Grafted $CaAl_{12}O_{19}:Mn^{4+}$ Color-Tunable Hybrid Phosphor. *Adv. Opt. Mater.* **2016**, *4*, 427−434.

(18) Wang, B.; Lin, H.; Huang, F.; Xu, J.; Chen, H.; Lin, Z.; Wang, Y. Non-Rare-Earth $BaMgAl_{10-2x}O_{17}:xMn^{4+},xMg^{2+}$: A Narrow-Band Red Phosphor for Use as a High-Power Warm w-LED. *Chem. Mater.* **2016**, *28*, 3515−3524.

(19) Singh, S. P.; Kim, M.; Park, W. B.; Lee, J.-W.; Sohn, K.-S. Discovery of a Red-Emitting $Li_3RbGe_8O_{18}:Mn^{4+}$ Phosphor in the Alkali-Germanate System: Structural Determination and Electronic Calculations. *Inorg. Chem.* **2016**, *55*, 10310−10319.

(20) Lin, C. C.; Meijerink, A.; Liu, R.-S. Critical Red Components for Next-Generation White LEDs. *J. Phys. Chem. Lett.* **2016**, *7*, 495−503.

(21) Sijbom, H. F.; Joos, J. J.; Martin, L. I. D. J.; Van den Eeckhout, K.; Poelman, D.; Smet, P. F. Luminescent Behavior of the $K_2SiF_6:Mn^{4+}$ Red Phosphor at High Fluxes and at the Microscopic Level. *ECS J. Solid State Sci. Technol.* **2016**, *5*, R3040−R3048.

(22) Tang, F.; Su, Z.; Ye, H.; Wang, M.; Lan, X.; Phillips, D. L.; Cao, Y.; Xu, S. A set of manganese ion activated fluoride phosphors ($A_2BF_6:Mn^{4+}$, A=K, Na, B=Si, Ge, Ti): synthesis below 0 °C and efficient room-temperature photoluminescence. *J. Mater. Chem. C* **2016**, *4*, 9561−9568.

(23) See for example, a recent review and references therein. Nguyen, H.-D.; Liu, R.-S. Narrow-band red-emitting Mn^{4+}-doped hexafluoride phosphors: synthesis, optoelectronic properties, and applications in white light-emitting diodes. *J. Mater. Chem. C* **2016**, *4*, 10759−10775.

(24) Tang, F.; Su, Z.; Ye, H.; Xu, S.; Guo, W.; Cao, Y.; Gao, W.; Pan, X. Boosting phonon-induced luminescence in red fluoride phosphors via composition-driven structural transformations. *J. Mater. Chem. C* **2017**, *5*, 12105−12111.

(25) Tang, F.; Ye, H.; Su, Z.; Bao, Y.; Guo, W.; Xu, S. Luminescence Anisotropy and Thermal Effect of Magnetic and Electric Dipole Transitions of Cr^{3+} Ions in Yb: YAG Transparent Ceramic. *ACS Appl. Mater. Interfaces* **2017**, *9*, 43790−43798.

(26) Hoshino, R.; Adachi, S. Optical spectroscopy of $ZnSiF_6 \cdot 6H_2O:Mn^{4+}$ red phosphor. *J. Appl. Phys.* **2013**, *114*, 213502.

(27) Henderson, B.; Imbusch, G. F. *Optical Spectroscopy of Inorganic Solids*; Oxford University Press: U.K. Oxford, 1989.

(28) Sijbom, H. F.; Verstraete, R.; Joos, J. J.; Poelman, D.; Smet, P. F. $K_2SiF_6:Mn^{4+}$ as a red phosphor for displays and warm-white LEDs: a review of properties and perspectives. *Opt. Mater. Express* **2017**, *7*, 3332−3365.

(29) Wei, L.-L.; Lin, C. C.; Fang, M.-H.; Brik, M. G.; Hu, S.-F.; Jiao, H.; Liu, R.-S. A low-temperature co-precipitation approach to synthesize fluoride phosphors $K_2MF_6:Mn^{4+}$ (M=Ge, Si) for white LED applications. *J. Mater. Chem. C* **2015**, *3*, 1655−1660.

(30) Huang, L.; Zhu, Y.; Zhang, X.; Zou, R.; Pan, F.; Wang, J.; Wu, M. HF-Free Hydrothermal Route for Synthesis of Highly Efficient Narrow-Band Red Emitting Phosphor $K_2Si_{1-x}F_6:xMn^{4+}$ for Warm White Light-Emitting Diodes. *Chem. Mater.* **2016**, *28*, 1495−1502.

(31) Kasa, R.; Adachi, S. Red and deep red emissions from cubic $K_2SiF_6:Mn^{4+}$ and hexagonal K_2MnF_6 synthesized in $HF/KMnO_4/KHF_2/Si$ solutions. *J. Electrochem. Soc.* **2012**, *159*, J89−J95.

(32) Bersuker, I. B. *Electronic Structure and Properties of Transition Metal Compounds: Introduction to the Theory*, 2nd ed.; Wiley, 2010.

(33) Martin, T. P.; Fowler, W. B. Temperature dependence of phonon-induced electronic transitions in insulating solids. *Phys. Rev. B: Condens. Matter Mater. Phys.* **1970**, *2*, 4221−4225.

(34) Segall, B.; Mahan, G. D. Phonon-assisted recombination of free excitons in compound semiconductors. *Phys. Rev.* **1968**, *171*, 935−948.

(35) Xu, S. J.; Li, G. Q.; Xiong, S.-J.; Che, C. M. Temperature dependence of the LO phonon sidebands in free exciton emission of GaN. *J. Appl. Phys.* **2006**, *99*, 073508.

(36) Suna, A. Green's Function Approach to Exciton-Phonon Interactions. *Phys. Rev.* **1964**, *135*, A111−A123.

(37) Orgel, L. E. *An Introduction to Transition Metal Chemistry. Ligand field theory*, 2nd ed.; Methuen and Co., Ltd.: Great Britain, 1966; p 94.

(38) Wall, W. A.; Karpick, J. T.; Bartolo, B. D. Temperature dependence of the vibronic spectrum and fluorescence lifetime of $YAG:Cr^{3+}$. *J. Phys. C: Solid State Phys.* **1971**, *4*, 3258−3264.

(39) Katayama, Y.; Viana, B.; Gourier, D.; Xu, J.; Tanabe, S. Photostimulation induced persistent luminescence in $Y_3Al_2Ga_3O_{12}:Cr^{3+}$. *Opt. Mater. Express* **2016**, *6*, 1405−1413.

(40) Fischer, G. *Vibronic Coupling: The Interaction between the Electronic and Nuclear Motions*; Academic Press: New York, 1984.

(41) Curie, D. *Luminescence in Crystals*; Methuen and Co., Ltd.: Great Britain, 1963.

(42) Haddy, A. EPR spectroscopy of the manganese cluster of photosystem II. *Photosynth. Res.* **2007**, *92*, 357−368.

(43) Murata, T.; Tanoue, T.; Iwasaki, M.; Morinaga, K.; Hase, T. Fluorescence properties of Mn^{4+} in $CaAl_{12}O_{19}$ compounds as red-emitting phosphor for white LED. *J. Lumin.* **2005**, *114*, 207−212.

(44) https://www.lumileds.com/products/midpower-leds/luxeon-3535l.

(45) Guo, W.; Banerjee, A.; Bhattacharya, P.; Ooi, B. S. InGaN/GaN disk-in-nanowire white light emitting diodes on (001) silicon. *Appl. Phys. Lett.* **2011**, *98*, 193102.

(46) Philip, M. R.; Choudhary, D. D.; Djavid, M.; Bhuyian, M. N.; Piao, J.; Pham, T. T.; Misra, D.; Nguyen, H. P. T. Controlling color emission of InGaN/AlGaN nanowire light-emitting diodes grown by molecular beam epitaxy. *J. Vac. Sci. Technol., B: Nanotechnol. Microelectron.: Mater., Process., Meas., Phenom.* **2017**, *35*, 02B108.

(47) Philip, M. R.; Choudhary, D. D.; Djavid, M.; Bhuyian, M. N.; Bui, T. H. Q.; Misra, D.; Khreishah, A.; Piao, J.; Nguyen, H. D.; Le, K. Q.; Nguyen, H. P. T. Fabrication of Phosphor-Free III-Nitride Nanowire Light-Emitting Diodes on Metal Substrates for Flexible Photonics. *ACS Omega* **2017**, *2*, 5708−5714.